

See discussions, stats, and author profiles for this publication at: <https://www.researchgate.net/publication/231647832>

# Characterization of a New Solid Having Graphitic Hexagonal Pores with a GCMC Technique

ARTICLE *in* THE JOURNAL OF PHYSICAL CHEMISTRY C · JUNE 2011

Impact Factor: 4.77 · DOI: 10.1021/jp203264x

---

CITATIONS

14

READS

14

7 AUTHORS, INCLUDING:



[Phuong Thi Mac Nguyen](#)

University of Queensland

13 PUBLICATIONS 122 CITATIONS

[SEE PROFILE](#)



[Duong Do](#)

University of Queensland

493 PUBLICATIONS 9,805 CITATIONS

[SEE PROFILE](#)



[David Nicholson](#)

University of Queensland

294 PUBLICATIONS 4,489 CITATIONS

[SEE PROFILE](#)

# Characterization of a New Solid Having Graphitic Hexagonal Pores with a GCMC Technique

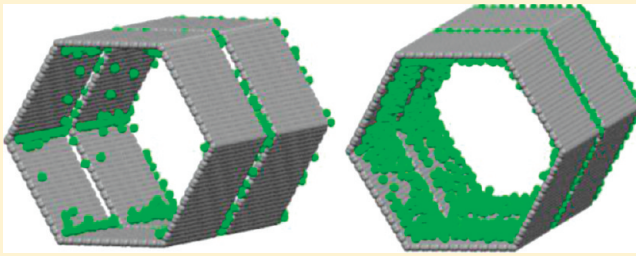
Yao Wang,<sup>†</sup> Phuong T. M. Nguyen,<sup>†</sup> Noriyuki Sakao,<sup>‡</sup> Toshihide Horikawa,<sup>†,‡</sup> D. D. Do,<sup>\*,†</sup> Kunimitsu Morishige,<sup>\*</sup> and D. Nicholson<sup>†</sup>

<sup>†</sup>School of Chemical Engineering, University of Queensland, St. Lucia, Qld 4072, Australia

<sup>‡</sup>Department of Advanced Materials, Institute of Technology and Science, The University of Tokushima, 2-1 minamijosanjima-cho, Tokushima 770-8506, Japan

<sup>\*</sup>Department of Chemistry, Okayama University of Science, 1-1 Ridai-cho, Kita-ku, Okayama 700-0005, Japan

**ABSTRACT:** Recently, Morishige (Morishige, K. Freezing and melting of Kr in hexagonally shaped pores of turbostratic carbon: Lack of hysteresis between freezing and melting. *J. Phys. Chem. C* 2011, 115 (6), 2720–2726) synthesized a new and exciting porous carbon material that has regular and nonconnected hexagonal pores with graphitic walls. Classical theories, such as the BJH or the DFT method, are unsuitable to characterize this material because the kernel (family of local isotherms) is based on model cylindrical pores. We present in this paper a new characterization based on a GCMC simulation of hexagonal pores that can account for the pore size, the surface morphology, and the heterogeneity arising from either structural or energetic defects. The molecular model describes the adsorption isotherms and the isosteric heat at 77.4 and 87.3 K over a wide range of pressures. This new material and the successful molecular model provide us with an ideal system to study adsorption mechanisms in a confined space, including the effects of confinement on the 2D transition for temperatures below the triple point and the 3D-capillary condensation for temperatures below the critical point of the bulk fluid.



## 1. INTRODUCTION

The recent discovery of highly ordered mesoporous materials, such as MCM-41 and SBA-15, has stimulated interest in capillary condensation and pore characterization. Because of the amorphous and heterogeneous surface of these silica materials, they are usually modeled by cylindrical channels with roughness or constriction properties.<sup>2–4</sup> They have also been modeled in a hexagonal shape in which heterogeneous surface properties are introduced by displacing O, Si, and H atoms randomly.<sup>4,5</sup> Because of their relatively large pore size and their inhomogeneous amorphous pore surfaces, these models can predict well the trend and shape of the experimental adsorption isotherm.

Recently, Morishige et al.<sup>1</sup> have synthesized a new carbonaceous porous material that has regular hexagonally shaped pores of the order of 9 nm in diameter. Their XRD results indicate that the walls are essentially graphitic, although there is no certainty that the walls are purely graphitic, and the detailed structure of the junctions between two walls remains a question for future research. To characterize this new material, a cylindrical model is no longer applicable because it does not carry any information about the junctions between two walls and cannot distinguish between hexagonal and cylindrical pore models. Therefore, in this study, we introduce a novel graphitic hexagonal pore model as a basis from which to estimate the pore size and explore theoretically the possibility of heterogeneity arising from either

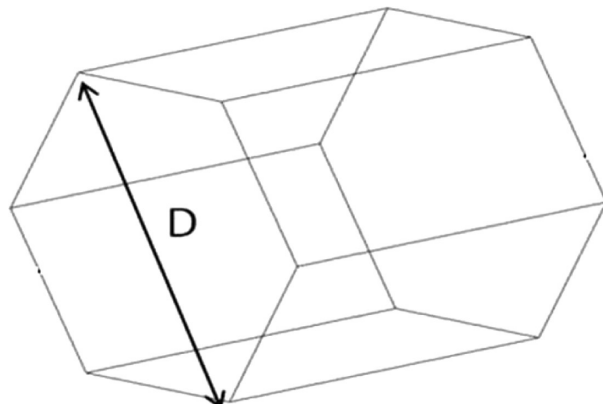


**Figure 1.** Schematic representation of the perfect hexagonal graphite model.

structural or energetic variation. Among many simulation and theoretical methods that have been applied to pore characterization with varying degrees of success, such as DFT, DS, SPE, Monte Carlo, and BM methods,<sup>7–12</sup> Monte Carlo simulation is

**Received:** April 8, 2011

**Revised:** May 22, 2011

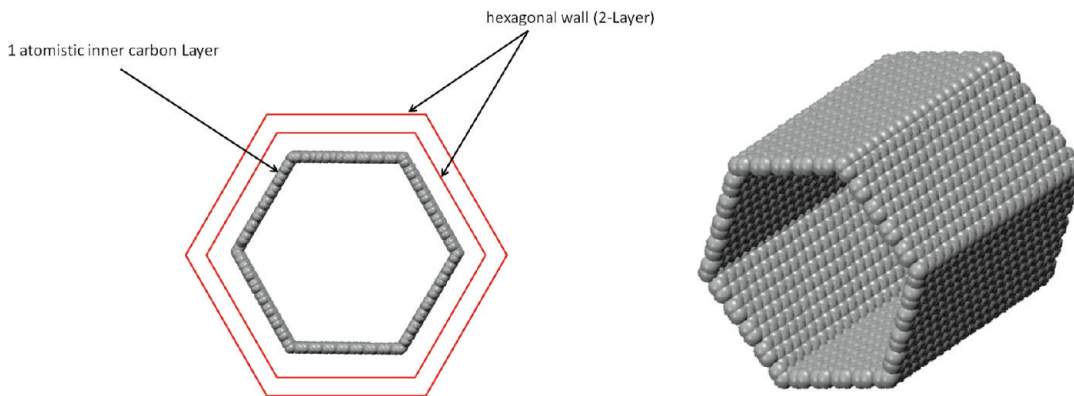


**Figure 2.** Schematic representation of the perfect hexagonal graphitic model.

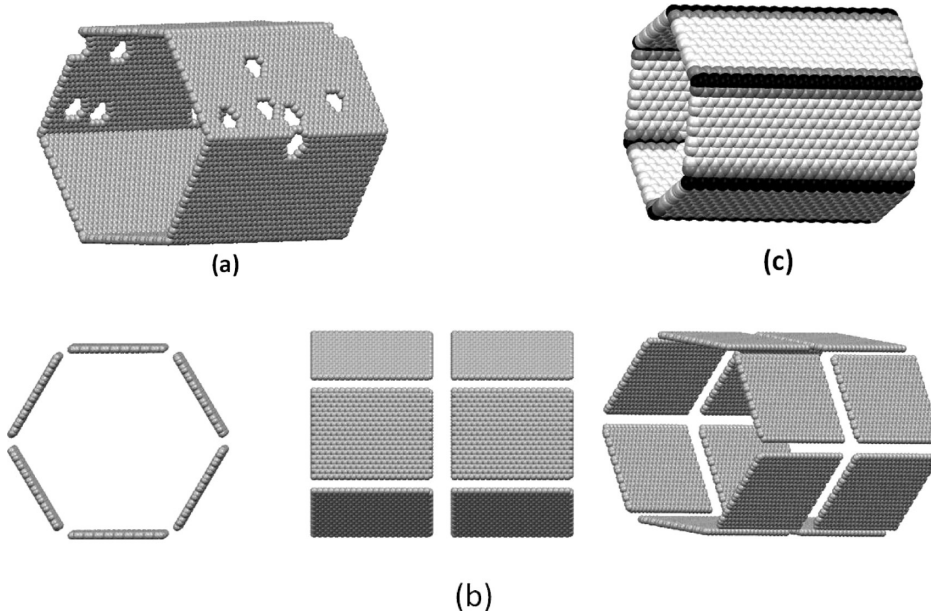


**Figure 3.** Schematic representation of the (a) structurally defective (with holes on the pore wall) hexagonal graphite model (only the atomistic inner pore wall is shown), (b) structurally defective (with separated patches) hexagonal graphite model (only the atomistic inner pore wall is shown), and (c) energetic defective (with strong sites at the vertexes of the pore) hexagonal graphite model.

chosen here to model the adsorption of argon in a hexagonal pore in which the pore morphology and pore heterogeneity can be modified.

In contrast to work reported elsewhere<sup>6</sup> in which only the pore size distribution of the material was explored, our work focuses on both pore size analysis and surface properties by analyzing the adsorption isotherm and the isosteric heat of argon at different temperatures. Because the physical behaviors, such as shape of the isotherm, the isosteric heat, and the condensation pressure of adsorption, are sensitive to the topology and morphology of the pore, the development of this new material will result in many interesting characteristics of adsorption that clearly distinguish this material from other solids, such as nonporous adsorbents, and those with slit and cylindrical pores. Both experimental and computational adsorption techniques have been used to characterize this material. We have studied both adsorption isotherms and isosteric heats and compare the simulated data with experiment, using argon as the molecular probe because it is spherical and nonspecific.

## 2. EXPERIMENTAL SECTION

**2.1. Material.** The highly ordered carbon material with hexagonally shaped pores was prepared by self-assembly of resorcinol-formaldehyde and Pluronic F127 triblock copolymer according to the procedure of Wang et al.<sup>13</sup> and carbonized at 2473 K for 1 h under argon atmosphere<sup>1</sup>

**2.2. Measurement.** Transmission electron microscopy (TEM) images were recorded on a JEOL JEM-2000EX electron microscope, operating at 200 kV. High-resolution adsorption isotherms of argon on prepared samples were measured at 77.4 K (boiling point of N<sub>2</sub> liquid) and 87.3 K (boiling point of Ar liquid) using the automatic volumetric adsorption apparatus (BELSORP-max, BEL Japan), in which three transducers with full scale ranges of 0.0133 kPa (0.1 Torr), 1.33 kPa (10 Torr), and 133 kPa (1000 Torr). The sample was heated to 473 K for 5 h under a turbo-molecular pump vacuum at pressures less than 0.1 mPa to clean its surface. We ensured that minute leakage of gases from the adsorption apparatus was avoided, using the checking system provided by BEL Japan.

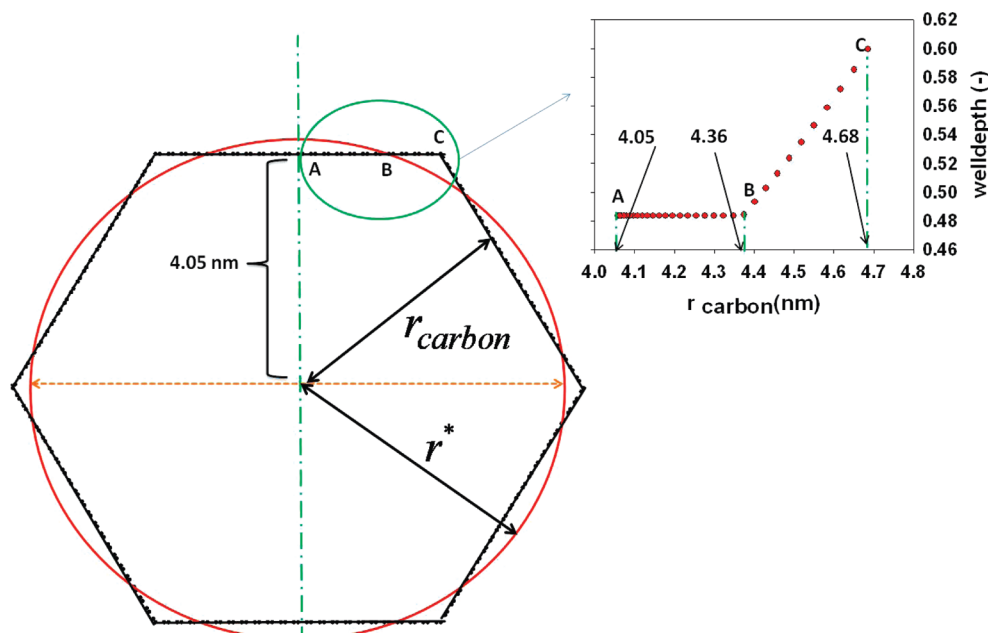


Figure 4. Schematic representation of how the energetic defects are created.

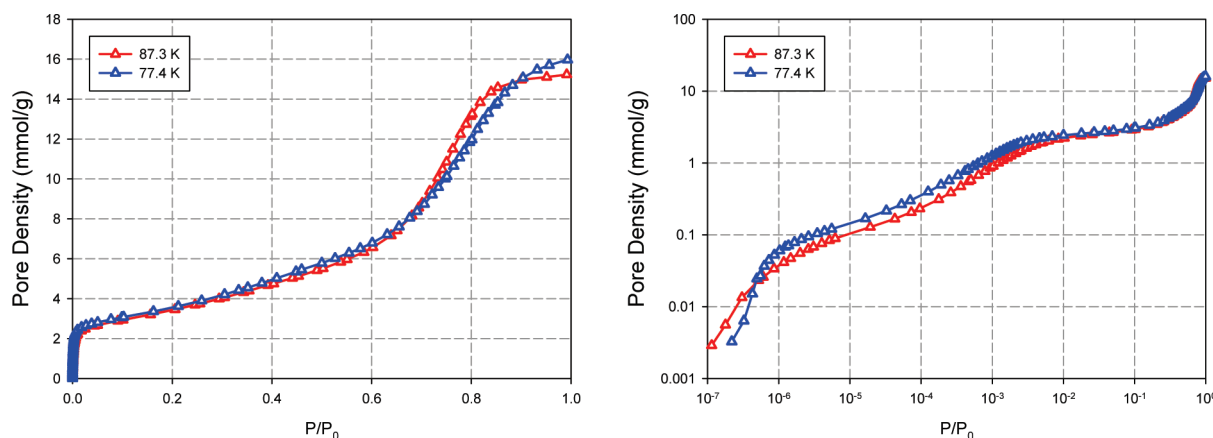


Figure 5. Experimental isotherms of argon adsorption at 77.4 and 87.3 K.

### 3. GCMC SIMULATION METHOD

The adsorption equilibrium was studied with the grand canonical Monte Carlo simulation (GCMC) using 30 000 cycles for the equilibrium and sampling stages. Each cycle consists of 1000 displacement moves and attempts to either insert or delete a particle with equal probability. The box lengths were set to twice the maximum pore width and periodic boundary conditions applied at the two boundaries in the axial direction to simulate a hexagonal pore of infinite extent. The cutoff radius was set to half the simulation box length. The displacement step length was initially set at half the simulation box length in the axial direction and then adjusted during the equilibration stage to achieve an acceptance ratio of the displacement move of between 20 and 25%.<sup>14</sup>

To describe the fluid–fluid interaction, we use the 12-6 Lennard-Jones equation with the following molecular parameters for argon:  $\sigma_{ff} = 0.3405$  nm and  $\epsilon_{ff}/k = 119.8$  K.<sup>15,16</sup>

**3.1. Pore Models.** The pore size of the hexagonally shaped pore ( $D$ ) is defined as the largest distance between two vertexes of the hexagon (see Figure 1).

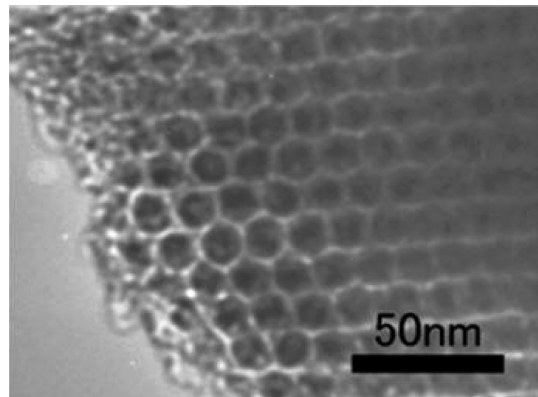


Figure 6. TEM image of the hexagonally shaped pore sample.<sup>1</sup>

We examined two kinds of models, described in detail in the next subsections. For the first one, we built the hexagonal pore by using unstructured walls. However, this model failed to reproduce

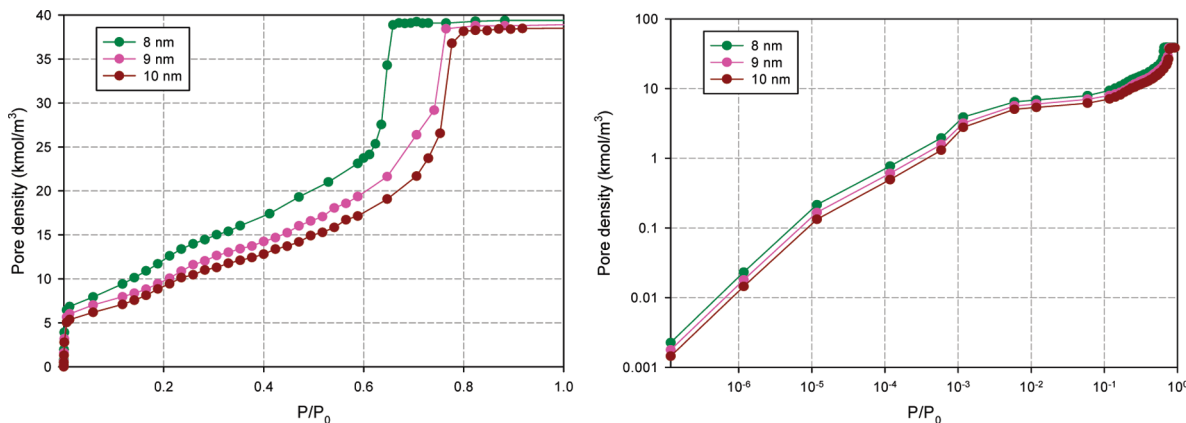


Figure 7. Simulation isotherms of argon adsorption at 87.3 K of pore sizes of 8.0, 9.0, and 10.0 nm.

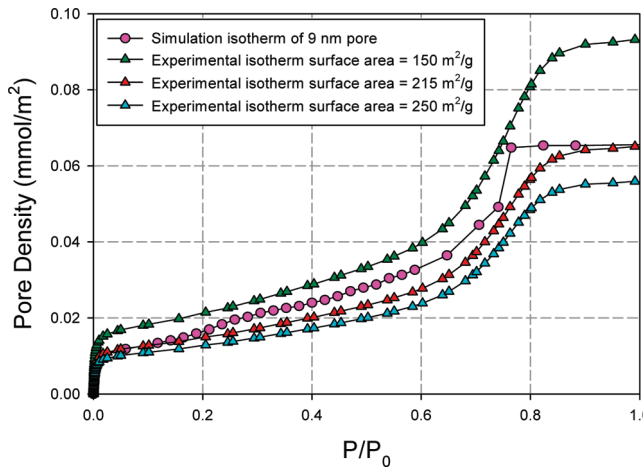


Figure 8. Simulation isotherm of argon adsorption at 87.3 K of pore sizes of 9.0 nm and experimental isotherms calculated with surface areas of 180, 215, and 250  $\text{m}^2/\text{g}$ .

the experimental isotherms in the low-pressure region (as discussed in section 4.1), and we concluded that a heterogeneous model was necessary. The second model (see section 3.1.2 below) was constructed from discrete carbon atoms for the innermost layer of the pore so that we can easily modify the structure to include structural and energetic variation.

In both models, the solid–fluid interaction parameters are obtained from the Lorentz–Berthelot rule

$$\sigma_{\text{sf}} = 0.5(\sigma_{\text{ss}} + \sigma_{\text{ff}}) \quad (1)$$

$$\varepsilon_{\text{sf}} = (\varepsilon_{\text{ss}} \varepsilon_{\text{ff}})^{1/2} \quad (2)$$

where  $\sigma_{\text{ss}}$  and  $\varepsilon_{\text{ss}}$  are the collision diameter and the well depth of interaction energy of a carbon atom ( $\sigma_{\text{ss}} = 0.34 \text{ nm}$  and  $\varepsilon_{\text{ss}}/k_{\text{B}} = 28 \text{ K}$ ).

**3.1.1. Unstructured Model.** In the unstructured model, the hexagonal pore is constructed from six finite strips modeled by a simple homogeneous (structureless) graphitized surface (Figure 1). The potential energy of the semi-infinite patches is calculated from the Bojan and Steele potential<sup>16–19</sup>

$$\varphi_{\text{f},\text{S}} = 2\pi(\rho_s \sigma_{\text{sf}}^2) \varepsilon_{\text{sf}} \{ [\varphi_{\text{rep}}(z, y^+) - \varphi_{\text{rep}}(z, y^-)] - [\varphi_{\text{att}}(z, y^+) - \varphi_{\text{att}}(z, y^-)] \} \quad (3)$$

where  $\rho_s$  is the surface density of the carbon center ( $38.2 \text{ nm}^{-2}$ ) and  $z$  is the distance from the surface to the argon particle. The other variables in the Bojan–Steele (BS) equation are  $y^+$  and  $y^-$ , which are described elsewhere.<sup>20</sup>

**3.1.2. Atomistic Model.** In the atomistic model, each surface of the innermost layer of the hexagonal pore is composed of carbon atoms arranged in a hexagon with a carbon–carbon bond length of 0.142 nm (Figure 2).

The outer layers are modeled as Bojan–Steele homogeneous surfaces, as described in the previous section. The structurally defective model of the hexagonal pore is constructed by two different methods: In the first (the common way to create graphite surface defects), a certain percentage of carbon atoms was removed to create strong site holes of 1 nm at which argon atoms can be housed<sup>21</sup> (shown in Figure 3a). The percentage of defects is the ratio between number of atoms removed and total number of atoms before removal. In this work, we chose values of defect percentage of 5, 15, and 30% and found that simulation data with 5% defects gave agreement between experimental and simulated isosteric heats (see section 4). A second approach is to model the basal plane surface on the basis of the XRD results,<sup>1</sup> which suggest that the graphite units are about 5 nm long in all directions. We used square patches of this size to construct the hexagonal pore, leaving a 1 nm gap between the patches, which act as strong sites for argon (Figure 3b).

Because it is reasonable to expect that the corner of the hexagonal pore contains energetically strong sites due to the displacement of electrons at the junctions, we also considered an energetic model. This model is achieved by allowing the surface strength to be highest at the junction of two basal planes and to decrease with distance away from the junction. The region away from the junction has the same surface strength as that of the graphene layer (Figure 3c). The diagram for the energetic variation is shown in Figure 4, where the well depth is varied with distance from the junction, according to the following equation

$$\varepsilon'_{\text{sf}} = \begin{cases} \varepsilon_{\text{sf}} \times \lambda^{(r_{\text{carbon}}/r^* - 1)} & (r_{\text{carbon}} \geq r^*) \\ \varepsilon_{\text{sf}} & (r_{\text{carbon}} < r^*) \end{cases} \quad (4)$$

where  $r_{\text{carbon}}$  refers to the distance of the carbon atom to the center of the pore and  $r^*$  is a parameter that defines the vertex

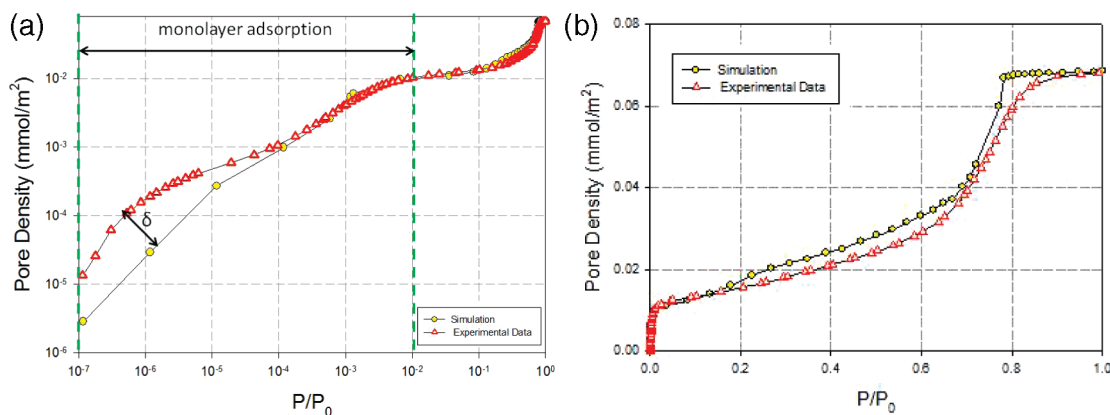


**Figure 9.** Experimental and simulated data for argon adsorption on the hexagonal pore model at 87.3 K. The surface area is adjusted as 205 m<sup>2</sup>/g. Panels: (a) log–log plot and (b) linear plot.

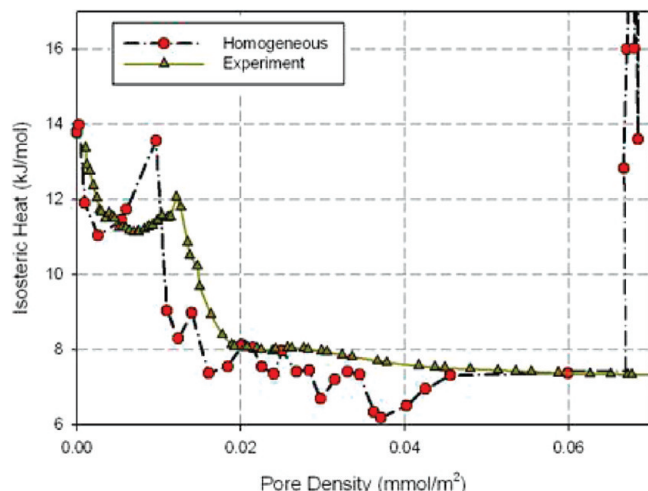


**Figure 10.** Isosteric heat of argon adsorption calculated from experimental data and in a 9.37 nm homogeneous graphitized carbon hexagonal pore.

area (shown in Figure 4). In this work, we used  $r^* = 4.36$  nm and  $\lambda = 20$ .

**3.2. Isosteric Heat.** The isosteric heat of adsorption is calculated in two different ways. The first uses adsorption isotherms at two nearby temperatures and the classical Clausius–Clapeyron equation<sup>22</sup>

$$q_{\text{iso}} = -R \frac{\ln P_2 - \ln P_1}{1/T_2 - 1/T_1} \quad (5)$$

where  $R$  is the gas constant,  $T_1$  and  $T_2$  are temperatures, and  $P_1$  and  $P_2$  are the pressures at which the surface excess of the two isotherms are the same. We applied this equation to calculate the isosteric heat of adsorption using experimental adsorption isotherms of argon at 77.4 and 87.3 K.

The second approach is to calculate the isosteric heat from a GCMC simulation by using the following equation, which can be derived from fluctuation theory<sup>23</sup>

$$Q = \Delta \bar{h}_{\text{ex}} = \frac{f(U, N)}{f(N, N) - f(N_G, N_G)} - \frac{N_G k_B T}{f(N_G, N_G)} \quad (6)$$

where  $N$  and  $N_G$  are the numbers of particles in the simulation box of the pore and the bulk phase box having the same volume as

the accessible volume of the adsorption system, respectively, and  $k_B$  is the Boltzmann constant.

The separate contribution of the solid–fluid interaction and the fluid–fluid interaction can be obtained from the first term on the RHS of eq 6 by replacing the total potential energy  $U$  by  $U_{\text{FF}}$  and  $U_{\text{SF}}$ , respectively, where  $U_{\text{FF}}$  is the fluid–fluid interaction energy and  $U_{\text{SF}}$  is the solid–fluid potential energy of the system.

#### 4. RESULTS AND DISCUSSION

The experimental isotherms of argon adsorption at 77.4 and 87.3 K are shown in Figure 5. The argon adsorption isotherm at 87.3 K shows a rather steep increase in the relative pressure range between 0.6 and 0.85. The log–log plot shows two regions of distinctly different slopes at the low loading region ( $P/P_0 = 10^{-7}$ – $10^{-6}$ ). This suggests that the surface might be less homogeneous than a graphitic carbon surface reported, for example, by Nakai et al.<sup>24</sup>

We calculated the pore size distribution from the argon adsorption isotherm at 87.3 using the NLDFT method with a graphitic cylindrical pore model to construct the kernel of local isotherms for pores of different sizes. The PSD is very sharp, and the mean pore size was found to be ca. 9 nm. However, this result cannot be regarded as being reliable, because the pores are hexagonal rather than cylindrical. In addition, the TEM image (Figure 6) shows that the pore shape is hexagonal and the pore size is ca. 10 nm.<sup>1</sup> We, therefore, simulated isotherms of 8.0, 9.0, and 10.0 nm pores by using the homogeneous unstructured model of hexagonal pores to compare with the experimental data, and the results are shown in Figure 7.

From Figures 7 and 5, the condensation pressure ( $P/P_0 = 0.75$ ) of the 9 nm pore is very close to the experimental data, although the simulated isotherm exhibits a steeper condensation. We also determined the surface area by matching the saturation capacity of the 9 nm pore to that of the experimental data by changing the surface area and find that the surface area of 215 m<sup>2</sup>/g gives the best agreement between experimental and simulated isotherms (Figure 8).

To make the pore size approximation more realistic, the atomistic model was used. Because this model is constrained by the integral number of hexagons in graphite, only certain pore sizes can be constructed. Thus, we can construct three pore sizes

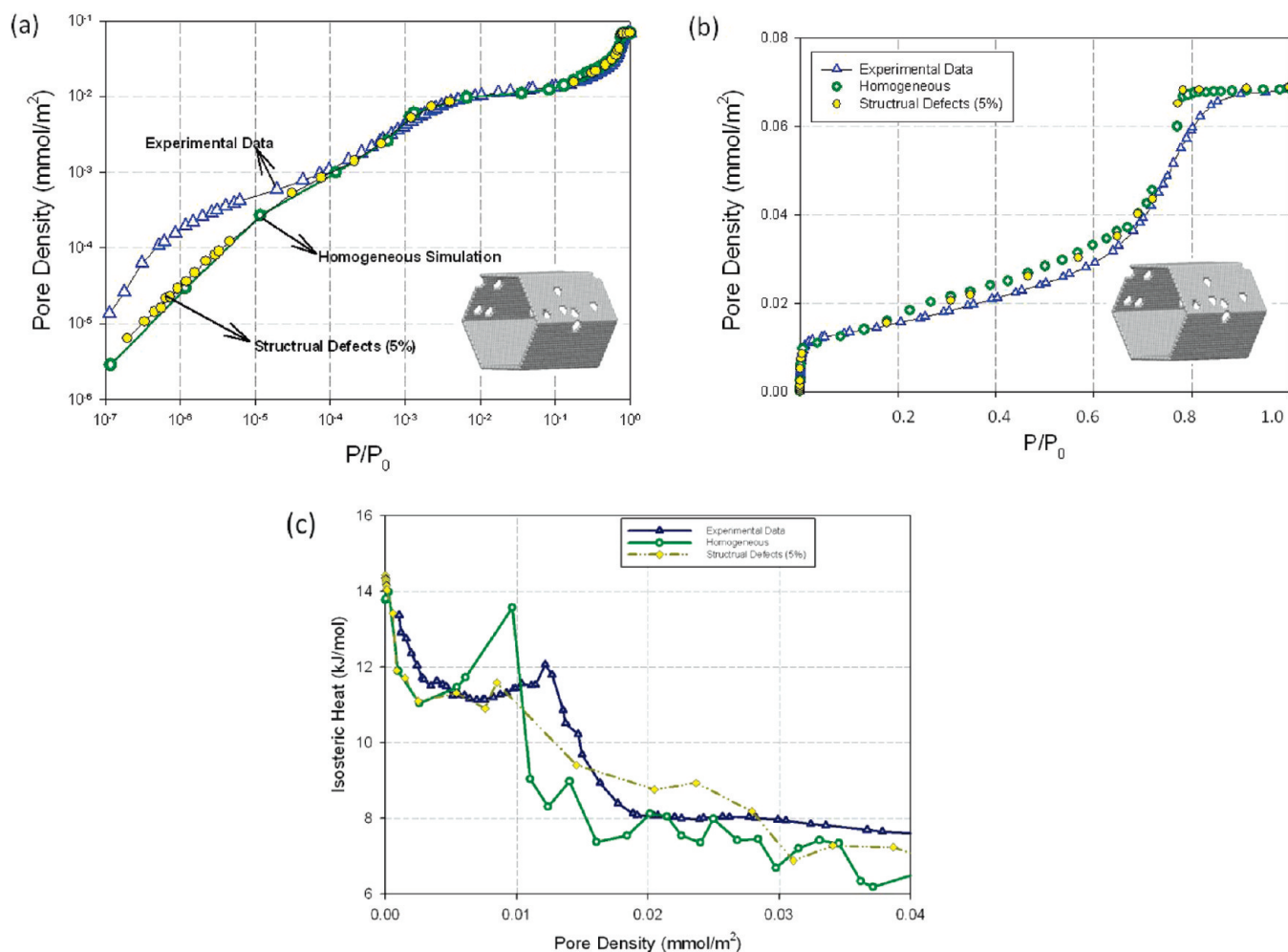


**Figure 11.** Comparison between experimental data (blue diamond) and two different simulation results for argon adsorption at 87.3 K. The simulation results are the homogeneous model (green open circle) and the structural defective model (yellow solid circle). Panels: (a) log–log isotherm, (b) linear isotherm, and (c) isosteric heat.

for a hexagonal pore using the atomistic model of around 9 nm in size: 8.52, 9.37, and 10.22 nm. We chose 9.37 nm as being closest to 9 nm. We also determined the surface area by matching the saturation capacity of the 9.37 nm pore to that of the experimental data and acquire the value of  $205 \text{ m}^2/\text{g}$  (shown in Figure 9b). That this value of surface area is lower than the BET surface area ( $263 \text{ m}^2/\text{g}$ )<sup>1</sup> confirms that the surface area obtained by GCMC is different from the BET surface area from experiment.<sup>25</sup>

**4.1. Homogeneous Hexagonal Pore Model.** We start the characterization by applying the homogeneous model to explore whether the simulated isotherm and isosteric heat agree with experimental data. If a good agreement can be found, then the homogeneous model is a good candidate to describe the experimental system. However, if not, we need to consider the heterogeneous models described in section 3.1.2.

In Figure 9, we compare our simulated isotherm with the experimental data of argon adsorption on this material at 87.3 K. The low-pressure region of the isotherm is displayed in Figure 9a as a log–log plot. The comparison of these isotherms shows that the simulated isotherm exhibits the same pattern as the experimental isotherm in the multilayer

region (Figure 9b). Although the simulated isotherm can reproduce the adsorption of argon on this hexagonal porous material fairly well, the fit is still poor in the monolayer region (Figure 9a), which can be attributed to the structural or energetic differences between the real material and the homogeneous model.

To illustrate further the failure of the homogeneous model in the monolayer region, we compare the simulated isosteric heat with the experimental isosteric heat. Figure 10 shows the isosteric heat obtained from the homogeneous model and the Clausius–Clapeyron experimental heat at 77.4 and 87.3 K. We notice that the discrepancy between our simulated curve and the experimental one is mainly shown in the monolayer region ( $0$ – $0.015 \text{ mmol}/\text{m}^2$ ), in agreement with our analysis of isotherms that the surface is not homogeneous.

**4.2. Heterogeneous Models of Graphitic Hexagonal Pore.** We carried out simulations with the different heterogeneous models described in section 3.1.2 to compare with the experimental data. We first consider models containing only structural defects and energetic variation separately, and then we decide whether it is necessary to combine the structural and energetic variations to achieve a satisfactory model.

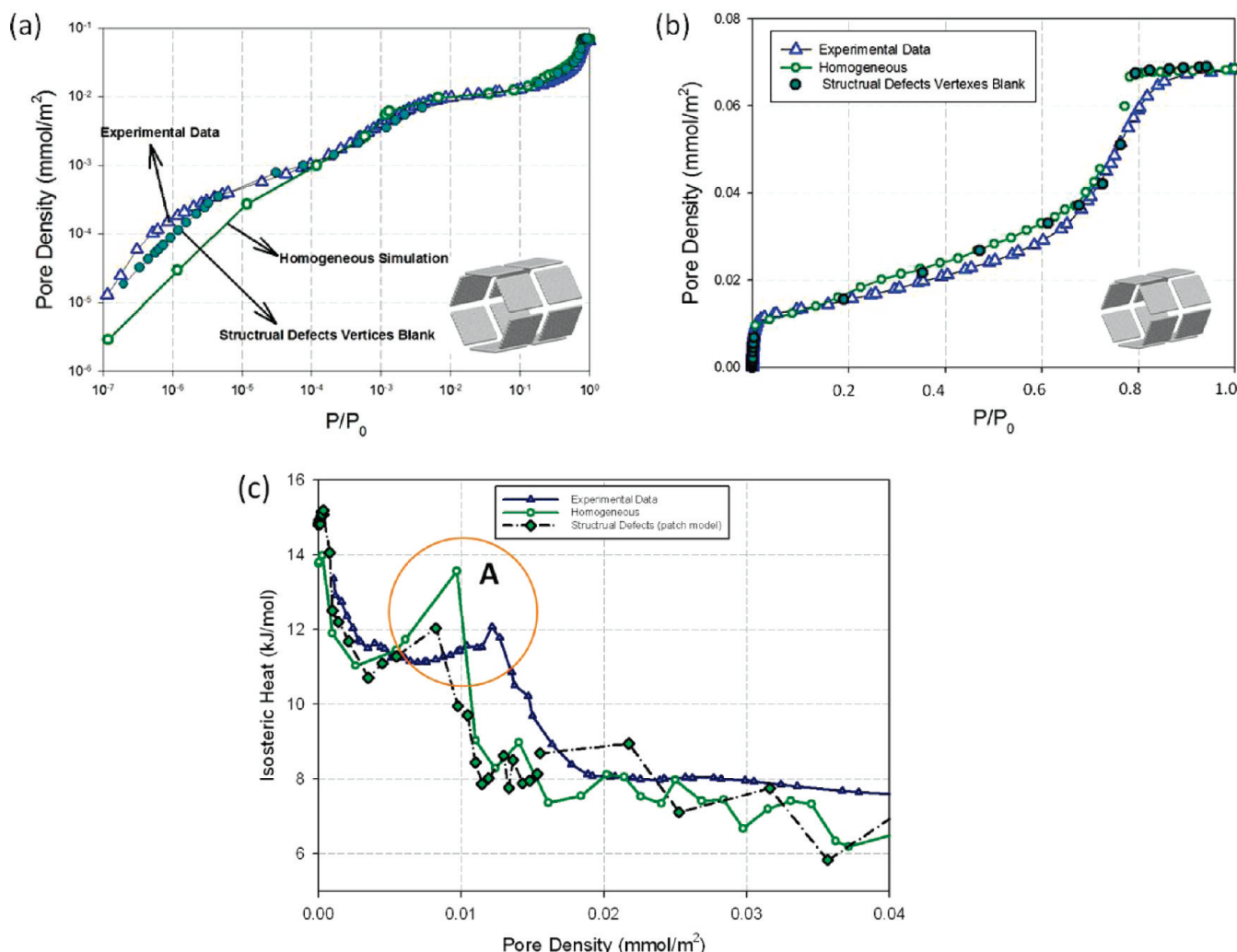


**Figure 12.** Comparison between experimental data (blue triangle) and two different simulation results. The simulation results are the homogeneous model (green open circle) and the patch structural defective model (green solid circle). The adsorption isotherms and the isosteric heat are for the adsorption of argon on a hexagonal pore at 87.3 K. Panels: (a) log–log isotherm, (b) linear isotherm, and (c) isosteric heat.

**4.2.1. Structural Heterogeneous Models. Structurally Defective Model.** This model is shown in Figure 3a (section 3.1.2). The adsorption isotherms and isosteric heat for the argon adsorption at 87.3 K for this model are compared with experimental data in Figure 11.

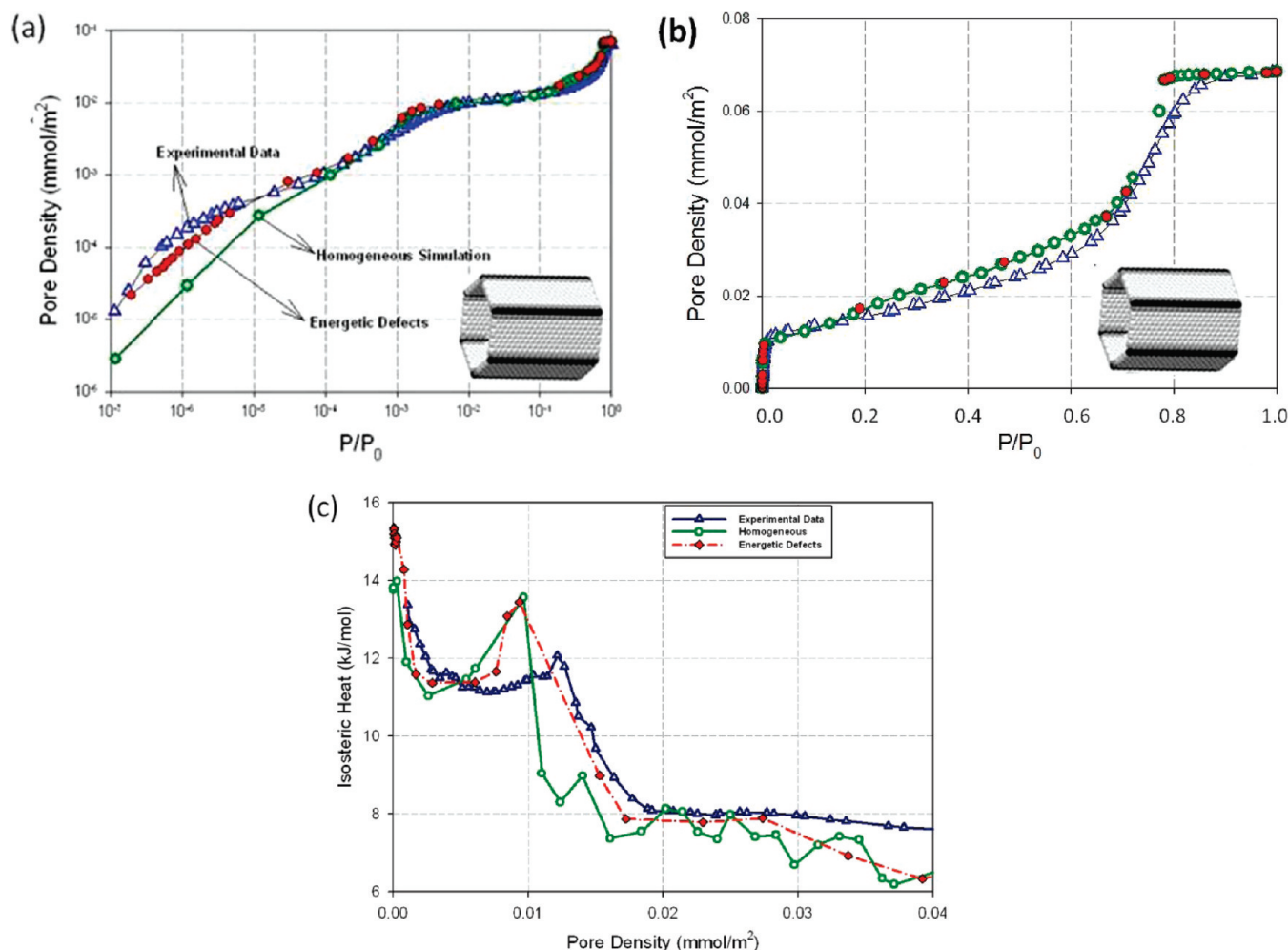
This figure also shows the simulation results from the homogeneous model to again highlight the deficiency of the homogeneous model and illustrate how the heterogeneous model will help to resolve these deficiencies. First, the isotherm obtained from this “defective model” exhibits the same trend as the homogeneous model in the multilayer region. This suggests that the capillary condensation pressure is not influenced by the pore wall irregularity mainly because the solid–fluid interactions are short-ranged.<sup>5</sup>

Figure 11a shows that, even when we introduce defects in the graphene layer, the agreement between the simulation results of the defective model and the experimental data is still very poor in the monolayer region, as observed for both isotherm and isosteric heat, although we note that the isosteric heat for the defective model gives a better description of the data, but further improvement is desirable, especially in the description of the isotherm.

**Patch Model.** On the basis of the XRD results, we have proposed a “patch model” (section 3.1.2, Figure 3b). The percentage of defects is 16% using the same calculation method as for the structurally defective model in section 3.1.2. The adsorption isotherms and isosteric heat of argon at 87 K for the patch model are shown in Figure 12 in comparison with experimental data along with the simulation results of the homogeneous model.

The patch model clearly outperforms the homogeneous model in the description of both isotherm and isosteric heat data in the monolayer region and lends support to the patch nature of the pore wall as characterized by X-ray diffraction, although the loading at which the heat maximum is observed (region A) is lower than that observed experimentally and suggests that further improvement to the modeling is called for.

**4.2.2. Energetic Heterogeneous Model.** To further improve the description of isosteric heat versus loading, we consider the model with a modified energy parameter (see section 3.1.2 for a detailed description). The adsorption isotherm and the isosteric heat of this model are shown in Figure 13 in



**Figure 13.** Comparison between experimental data (blue triangle) and two different simulation results. The simulation results are the homogeneous model (green open circle) and the energetic defective model (red solid circle). The adsorption isotherms and the isosteric heat are for the adsorption of argon on a hexagonal pore at 87.3 K. Panels: (a) log–log isotherm, (b) linear isotherm, and (c) isosteric heat.

comparison with the homogeneous model and the experimental data.

Clearly, the energetic model is an improvement on the homogeneous model, especially the description of the isosteric heat in the multilayer region.

**4.2.3. Composite Model.** The modeling described in the earlier sections strongly suggests that a model incorporating energetic heterogeneity is necessary to account for the experimental data. The patch model and the energetic model both give good descriptions of the isotherm, whereas the defective model describes the isosteric heat better. This leads us to propose a composite model, which accounts for the energetic variation at the corners with each surface of the hexagonal pore composed of patches separated from each other by a 1 nm gap, as suggested by the XRD results. The simulated isotherm and the isosteric heat versus loading for this composite model are shown in Figure 14 together with the experimental data.

To confirm that the chosen model is appropriate, we have simulated the adsorption isotherm of argon at 77.4 K and compared it with experimental data. It can be seen in Figure 15 that the composite model gives a good description of the isotherm (plotted against the reduced pressure,  $P/P_0$ ) and

lends strong support to this model as a predictive tool to investigate adsorption on this adsorbent at various temperatures. Because 77.4 K is below the triple point, the saturation vapor pressures  $P_0$  used in the simulation results and the experimental data are obtained by extrapolating (i.e., supercooled liquid) the corresponding vapor pressures in the vapor–liquid coexistence range by using the Antoine equation.<sup>26</sup> For simulation, this saturation vapor pressure is 24.7 kPa, whereas that for experimental data is 30.9 kPa.<sup>27</sup>

**4.3. Microscopic Behavior of Argon Adsorption in the Hexagonal Pore.** To have a better insight of argon adsorption at 87.3 K in the hexagonal pore, we compare adsorption isotherms of (1) the composite model, (2) the homogeneous model, and (3) the flat graphitic surface in Figure 16.

Figure 16a shows that the adsorption density calculated from the homogeneous hexagonal pore is higher than that for the flat surface in the monolayer region. This difference is due to the corner effects of the hexagonally shaped pore in which an argon atom in the neighborhood of the corner has more adsorbent atoms at closer separation distances (Figure 17a,b), resulting in a greater solid–fluid potential compared to that of the flat graphitic surface. Not only is there a greater solid–fluid potential

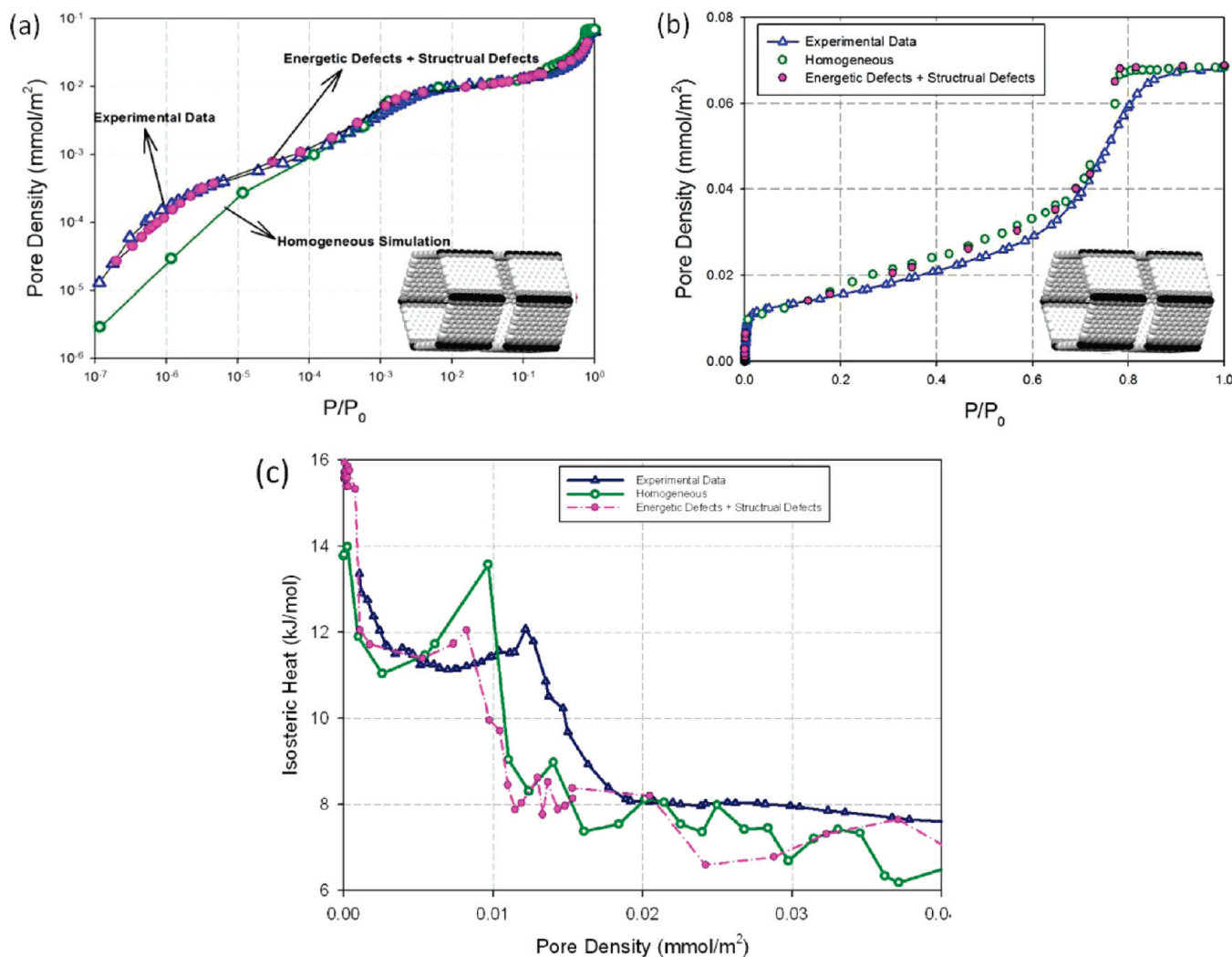


**Figure 14.** Comparison between experimental data (blue triangle) and two different simulation results. The simulation results are the homogeneous model (green open circle) and the structural and energetic defective model (magenta solid circle). The adsorption isotherms and the isosteric heat are for the adsorption of argon on a hexagonal pore at 87.3 K. Panels: (a) log–log isotherm, (b) linear isotherm, and (c) isosteric heat.

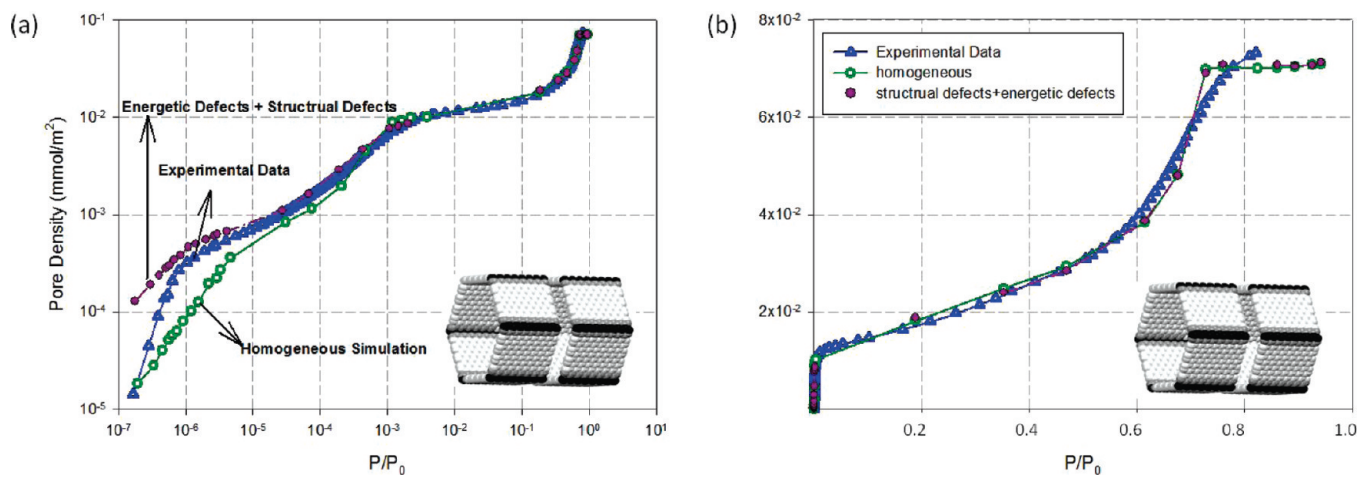
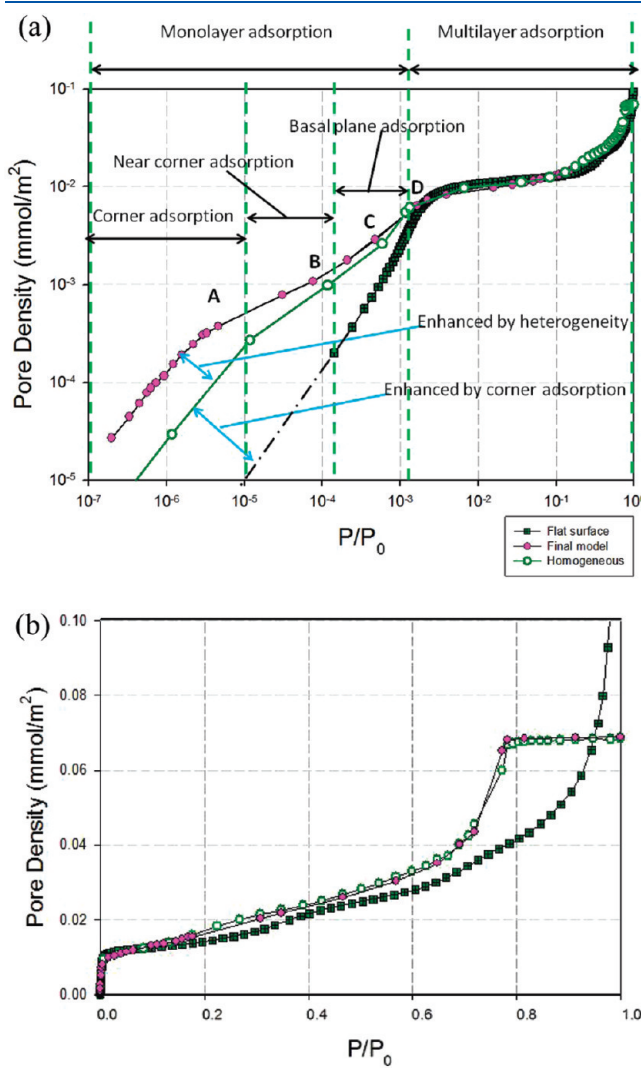


**Figure 15.** Experimental and simulation isotherms for argon adsorption on a hexagonal pore model at 77.4 K: (a) log–log plot and (b) linear plot.

but also the fluid–fluid interaction is enhanced in comparison to adsorption on a flat surface because of the closer separation

between an adsorbate and its nearest-neighboring particles and also because of the greater well depth of carbon atoms at the

junctions joining the two walls (Figure 17a,c). This enhancement of the hexagonal pore has also been studied in MCM-41 by Ustinov.<sup>28</sup> Figure 16a also shows that the composite model gives a greater loading than the homogeneous model in the low loading region, and this is due to the energetic and structural heterogeneity.



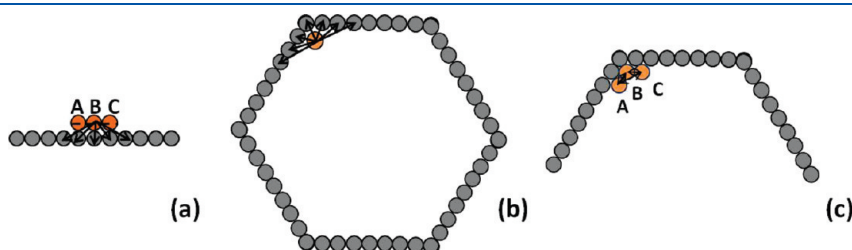
**Figure 16.** Comparison between the flat surface isotherm (black square) and two different simulation isotherms. The simulation results are the homogeneous model (green open circle) and our final model (magenta solid circle) for the hexagonal pore. The adsorption isotherms are for the adsorption of argon at 87.3 K. Panels: (a) log–log isotherm and (b) linear isotherm.

Figure 18 shows the evolution of the first adsorption layer. At the very beginning of adsorption (from the zero loading to point A in Figure 16a), the argon particles are adsorbed along the six vertexes as well as in the gap between the patches. This is because argon particles can interact with a larger number of solid atoms (Figure 18A). The adsorption isotherm is linear in this region, and the slope is merely the affinity of the vertex.

As the vertexes of the hexagonal pore are occupied with more argon particles, the fluid–fluid interaction increases but the solid–fluid decreases because argon particles now begin to occupy the lower-energy sites of the basal plane, reducing the slope of the isotherm below unity (Figure 18B). As adsorption progresses further, argon adsorbs onto the basal plane and the adsorption isotherm is linear but its slope is now the affinity of the basal plane. This continues until the basal plane is covered with adsorbate (Figure 18C,D). After the first layer has been nearly completed, adsorption occurs in higher layers where the solid–fluid interaction is weaker and the dominant force of adsorption comes from the fluid–fluid interaction. Therefore, as the higher layers fill, there is not much difference between the isotherms calculated from the composite model and the homogeneous model. Finally, there is a jump in density corresponding to the capillary condensation inside the pore.

## 5. CONCLUSION

We have characterized for the first time a new graphitic porous solid with hexagonally shaped pores by comparing the isotherms and isosteric heats of adsorption from experiment with the grand canonical Monte Carlo (GCMC) simulation. To explore the surface characteristics of the material, we have developed four different models for the hexagonal pore: one homogeneous model and three heterogeneous models. The structurally defective model contains two kinds of defects: one with holes on the basal plane and the other with separated graphite patches. The third heterogeneous model has energetic variation in the neighborhood of corners. We found that none of the heterogeneous models with only one kind of heterogeneity is satisfactory. Therefore, we propose a model for this material by combining both the structural and the energetic variations in a composite model. This composite model is able to describe the experimental isotherm and isosteric heat of argon adsorption at 87.3 K and at 77.4 K and has the potential for the characterization of this family of graphitic porous materials with a hexagonal shape and for the prediction of adsorption isotherms and isosteric heats of different adsorbates over a wide range of temperatures.



**Figure 17.** Schematic diagram of gas adsorption inside a hexagonal pore and on the surface.

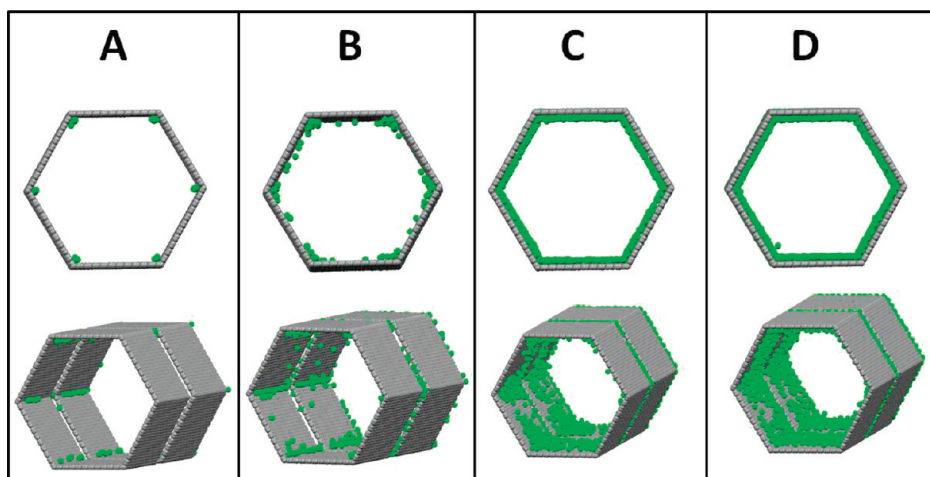


**Figure 18.** Snapshots of argon adsorption at 87.3 K for our final hexagonal pore model at different pressures (A–D are as labeled in Figure 16a).

## AUTHOR INFORMATION

### Corresponding Author

\*Fax: +61-7-3365-2789. E-mail: d.d.do@uq.edu.au.

## ACKNOWLEDGMENT

This project is supported by the Australian Research Council. We acknowledge the CSC for financial support in the form of a scholarship to Y.W. We also acknowledge the JSPS for its financial support in the form of the Excellent Young Researcher Overseas Visit Program to T.H.

## REFERENCES

- (1) Morishige, K. Freezing and melting of Kr in hexagonally shaped pores of turbostratic carbon: lack of hysteresis between freezing and melting. *J. Phys. Chem. C* **2011**, *115* (6), 2720–2726.
- (2) Puibasset, J. L. Monte-Carlo multiscale simulation study of argon adsorption/desorption hysteresis in mesoporous heterogeneous tubular pores like MCM-41 or oxidized porous silicon. *Langmuir* **2008**, *25* (2), 903–911.
- (3) Coasne, B.; Pellenq, R. J. M. Grand canonical Monte Carlo simulation of argon adsorption at the surface of silica nanopores: Effect of pore size, pore morphology, and surface roughness. *J. Chem. Phys.* **2004**, *120* (6), 2913–2922.
- (4) Coasne, B.; Hung, F. R.; Pellenq, R. J. M.; Siperstein, F. R.; Gubbins, K. E. Adsorption of simple gases in MCM-41 materials: The role of surface roughness. *Langmuir* **2006**, *22* (1), 194–202.
- (5) Palace Carvalho, A. J.; Ferreira, T.; Estêvão Candeias, A. J.; Prates Ramalho, J. P. Molecular simulations of nitrogen adsorption in pure silica MCM-41 materials. *J. Mol. Struct.: THEOCHEM* **2005**, *729* (1–2), 65–69.
- (6) Furmaniak, S.; Terzyk, A. P.; Jaroniec, M.; Gauden, P. A. Argon adsorption in channel-like mesoporous carbons at 77 K: Grand Canonical Monte Carlo simulations and pore size analysis. *Microporous Mesoporous Mater.* **2008**, *116* (1–3), 665–669.
- (7) Sunaga, M.; Ohba, T.; Suzuki, T.; Kanoh, H.; Hagiwara, S.; Kaneko, K. Nanostructure characterization of carbon materials with superwide pressure range adsorption technique with the aid of grand canonical Monte Carlo simulation. *J. Phys. Chem. B* **2004**, *108* (30), 10651–10657.
- (8) El-Merraoui, M.; Aoshima, M.; Kaneko, K. Micropore size distribution of activated carbon fiber using the density functional theory and other methods. *Langmuir* **2000**, *16* (9), 4300–4304.
- (9) Murata, K.; El-Merraoui, M.; Kaneko, K. A new determination method of absolute adsorption isotherm of supercritical gases under high pressure with a special relevance to density-functional theory study. *J. Chem. Phys.* **2001**, *114* (9), 4196–4205.
- (10) Murata, K.; Miyawaki, J.; Kaneko, K. A simple determination method of the absolute adsorbed amount for high pressure gas adsorption. *Carbon* **2002**, *40* (3), 425–428.
- (11) Ohba, T.; Kaneko, K. Internal surface area evaluation of carbon nanotube with GCMC simulation-assisted N<sub>2</sub> adsorption. *J. Phys. Chem. B* **2002**, *106* (29), 7171–7176.
- (12) Ohkubo, T.; Miyawaki, J.; Kaneko, K.; Ryoo, R.; Seaton, N. A. Adsorption properties of templated mesoporous carbon (CMK-1) for nitrogen and supercritical methane experiment and GCMC simulation. *J. Phys. Chem. B* **2002**, *106* (25), 6523–6528.
- (13) Wang, X.; Liang, C.; Dai, S. Facile synthesis of ordered mesoporous carbons with high thermal stability by self-assembly of resorcinol-formaldehyde and block copolymers under highly acidic conditions. *Langmuir* **2008**, *24* (14), 7500–7505.
- (14) Frenkel, D.; Smit, B. *Understanding Molecular Simulation: From Algorithms to Applications*; Academic Press: San Diego, 1996; Vol. xviii, p 443.
- (15) Do, D. D.; Do, H. D. Effects of potential models in the vapor–liquid equilibria and adsorption of simple gases on graphitized thermal carbon black. *Fluid Phase Equilif.* **2005**, *236* (1, 2), 169–177.
- (16) Bojan, M. J.; Steele, W. A. Computer simulation of physisorption on a heterogeneous surface. *Surf. Sci.* **1988**, *199* (3), L395–L402.
- (17) Bojan, M. J.; Steele, W. A. Computer simulations of the adsorption of xenon on stepped surfaces. *Mol. Phys.* **1998**, *95* (3), 431–437.
- (18) Bojan, M. J.; Steele, W. A. Computer simulation of physisorbed krypton on a heterogeneous surface. *Langmuir* **1989**, *5* (3), 625–633.
- (19) Bojan, M. J.; Steele, W. A. Computer simulation of physical adsorption on stepped surfaces. *Langmuir* **1993**, *9* (10), 2569–2575.
- (20) Fan, C.; Herrera, L. F.; Do, D. D.; Nicholson, D. New method to determine surface area and its energy distribution for nonporous solids: A computer simulation and experimental study. *Langmuir* **2010**, *26* (8), 5610–5623.
- (21) Wongkoblap, A.; Do, D. D. Characterization of carbot non-graphitized carbon blacks with a defective surface model: Adsorption of argon and nitrogen. *Carbon* **2007**, *45* (7), 1527–1534.
- (22) Do, D. D. *Adsorption Analysis: Equilibria and Kinetics*; Series on Chemical Engineering; Imperial College Press: London, 1998; p 892.
- (23) Do, D. D.; Do, H. D.; Nicholson, D. Molecular simulation of excess isotherm and excess enthalpy change in gas-phase adsorption. *J. Phys. Chem. B* **2009**, *113*, 1030–1040.
- (24) Nakai, K.; Yoshida, M.; Sonoda, J.; Nakada, Y.; Hakuman, M.; Naono, H. High resolution N<sub>2</sub> adsorption isotherms by graphitized carbon black and nongraphitized carbon black - $\alpha_s$ -curves, adsorption enthalpies and entropies. *J. Colloid Interface Sci.* **2010**, *351* (2), 507–514.

- (25) Do, D. D.; Do, H. D. Adsorption of argon on homogeneous graphitized thermal carbon black and heterogeneous carbon surface. *J. Colloid Interface Sci.* **2005**, *287* (2), 452–460.
- (26) Antoine, C. Tensions des vapeurs; nouvelle relation entre les tensions et les températures. *C. R. Séances Acad. Sci.* **1888**, *107*, 681–684, 778–780, 836–837.
- (27) Do, D. D.; Nicholson, D.; Do, H. D. Adsorption in micropores (nanopores): A computer appraisal of the Dubinin equations. *Mol. Simul.* **2009**, *35* (1), 122–137.
- (28) Ustinov, E. A. Modeling of N<sub>2</sub> adsorption in MCM-41 materials: Hexagonal pores versus cylindrical pores. *Langmuir* **2009**, *25* (13), 7450–7456.